ELSEVIER

Marine Geology 154 (1999) 211–226

MARINE GEOLOGY
INTERNATIONAL JOURNAL OF MARINE GEOLOGY, GEOCHEMISTRY AND GEOPHYSICS

The shallow porosity structure of the Eel shelf, northern California: results of a towed electromagnetic survey

Rob L. Evans [a,*], L.K. Law [b,1], B. St. Louis [c], S. Cheesman [d], K. Sananikone [e]

[a] *Department of Geology and Geophysics, Woods Hole Oceanographic Institution, Woods Hole, MA 02543, USA*
[b] *Pacific Geoscience Centre, North Saanich, BC V8L 4B2, Canada*
[c] *Geological Survey of Canada, Geophysics Division, Ottawa, ON K1A OY3, Canada*
[d] *Custom Geophysical Software, Toronto, ON, Canada*
[e] *Department of Earth Sciences, Texas A&M University, College Station, TX 77843, USA*

Received 13 March 1997; accepted 9 January 1998

Abstract

A towed electromagnetic survey, mapping the electrical resistivity of the seafloor, was conducted over an area of the Eel shelf off Humboldt Bay, California. Continuous resistivity profiles to 20 m below the seafloor were measured along 120 km of track line, from water depths of 100 m to around 30 m. The shallow structure along the shelf is highly variable and we identify three distinct environments based on the recorded resistivities and the porosities inferred from them. The first region is a mid-shelf depocenter, characterized by a thin (~2 m), moderately high-porosity (45–60%) surface layer, which overlies a less porous (35–45%) and homogeneous substrate, uniform both laterally and vertically. This region is found to the northwest of the Humboldt Bay entrance, from water depths of about 65 m to at least 100 m, and is roughly coincident with recent flood deposits. The second region is located closer to shore and contains extremely high resistivities for a shallow sedimentary environment. It reveals a high degree of spatial variability on length scales of several hundred meters. Several possibilities exist to explain such high resistivities and these include: upwelling fresh water channeled to the seafloor through local fault and anticline systems; a significant volume of natural gas within the sediments; or a continuous process of carbonate precipitation through oxidation of methane near the seafloor, which, over time, builds a substantial thickness of lithified material. None of the above explanations are mutually exclusive, and all could act in concert to increase resistivities. The third region roughly coincides with the Eel River delta and features a buried layer of moderately low porosity (30–35%) at a depth of about 5 m and with a thickness of between 5 and 10 m. This layer extends from near the entrance to Humboldt Bay in a southwesterly direction across the shelf.

Keywords: electromagnetic (EM); electrical resistivity; porosity; Eel River

* Corresponding author. E-mail: evans@hades.whoi.edu
[1] Retired.

0025-3227/99/$ – see front matter
PII: S0025-3227(98)00114-5

1. Introduction

The continental shelf near the Eel River, northern California has undergone many surveys of geological structure, defining the preserved strata, and of the local oceanographic environment, documenting the ongoing construction of shelf strata (Nittrouer and Kravitz, 1996; Nittrouer, 1999). The regional geology is dominated by tectonic activity associated with subduction of the Gorda Plate and the northward migration of the Mendocino triple junction (Field et al., 1987; Clarke, 1992). High-resolution sidescan imaging identified features that are controlled by the local ocean currents as well as by regional tectonics (Goff et al., 1999). In general, the shelf is flat and featureless, particularly its inner regions, due to terrigenous input that derives from the Eel River to the south and the Mad River to the north. However, the shelf bathymetry does reveal a vertical bulge associated with recent flood input (Goff et al., 1999). Also seen are areas of low acoustic backscatter associated with the Eel and Mad River deltas. The mid-shelf region is typically characterized by higher backscatter than these deltaic regions, at least to water depths of about 80 m (Borgeld et al., 1999).

Our contribution to the suite of experiments was a seafloor electromagnetic (EM) survey, measuring the electrical resistivity across the shelf. The motivation for using EM methods arises from a strong relationship between the amount and distribution of seawater in the seafloor and the bulk resistivity structure. Over sedimentary sequences, resistivity is a particularly useful parameter as it can be easily related to porosity and, from there, to grain size and texture.

Our survey featured 120 km of track lines across the shelf (Fig. 1) using a seafloor frequency-domain EM system (Fig. 2) developed by the Geological Survey of Canada. The system is a 50-m-long array that is dragged along the bottom. As the system is towed, it measures resistivity profiles to a depth of 20 m beneath the seafloor. The resistivity profiles measured along a track line can be interpreted in terms of sedimentary porosity, identifying structures with horizontal length scales on the order of 100 m. Thus, the technique is capable of identifying distinct facies on the shelf.

2. Resistivity of seafloor sediments

Within seafloor sediments, the electrical resistivity is dominated by seawater in interstices. This dependence arises because seawater has an electrical resistivity that is several orders of magnitude lower than that of the sedimentary matrix. If the seawater is distributed in a connected network, which is a good assumption except for the most indurated and diagenetically altered sedimentary sequences, then this network will provide the path of least resistance for electric current flow.

The electrical resistivity of sediments is most commonly related to porosity by Archie's law (Archie, 1942), which requires assumptions about the geometry of the fluid distribution. Archie's law (Fig. 3) can be written as:

$$\rho_{\mathrm{m}} = \rho_{\mathrm{f}} \phi^{-m}$$

where ρ_{m} is the measured resistivity, ρ_{f} is that of seawater, and ϕ is the porosity. The exponent m is a free parameter, but is typically about 1.4–1.5 for marine sands and increases as the grains become less spherical (Jackson et al., 1978). Based on resistor network analyses (Madden, 1976; Evans, 1994) and theoretical bounds on the resistivity of a two-phase medium (Hashin and Shtrikman, 1963; Schmeling, 1986) lower values of exponent, m, in Archie's law are related to a more connected or less tortuous fluid distribution within the sediment. As the porosity of sediments becomes larger, usually reflecting a transition to finer-grained or platey silts and clays, the appropriate exponent in Archie's law increases (in some cases exceeding 3.0; Jackson et al., 1978; Andrews and Bennett, 1984).

We have chosen an exponent of 1.8 to calculate apparent porosities, an appropriate value in formations of 50–60% porosity near the seafloor. At depth, or when porosity is ~40%, an exponent of 1.8 will over-predict porosity by 5%, and in this case a value of 1.4 is more appropriate. An exponent of 1.4 was the smallest value observed by Jackson et al. (1978) for marine sands, and so provides a reasonable lower bound on porosity.

The resistivity of seawater is a well understood function of temperature and salinity (Quist and Marshall, 1968; Perkin and Lewis, 1980; Nesbitt, 1993) and for normal seawater temperatures varies between

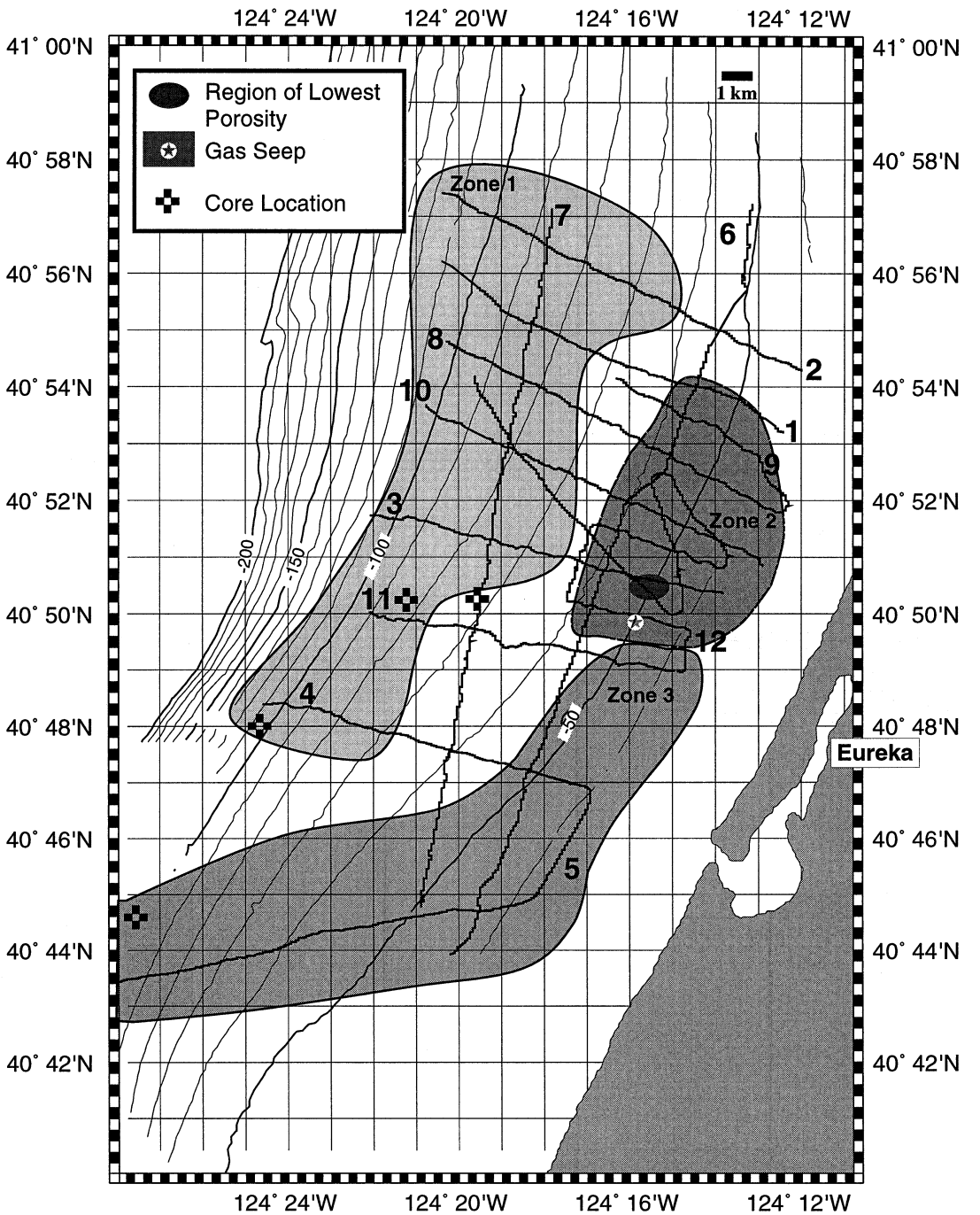

Fig. 1. A map of the survey area showing the 12 lines completed. The data delineate three regions of distinct porosity structure labelled *zones 1*, *2* and *3*, which are described in the text.

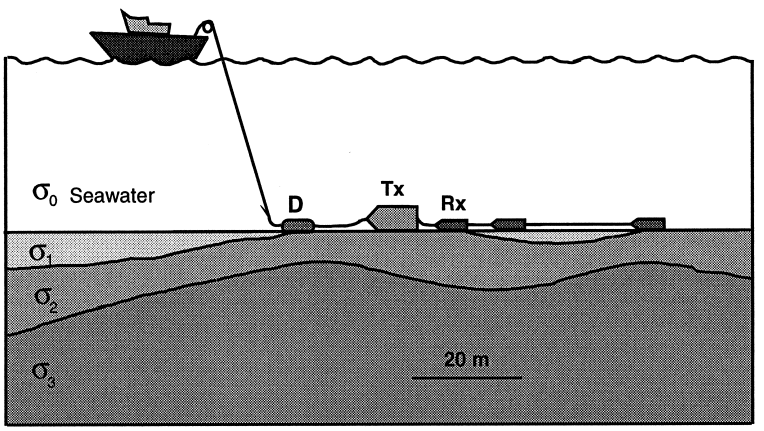

Fig. 2. A schematic of the towed electromagnetic system used for the survey. The system forms a 50-m-long array on the seafloor. The array consists of a depressor unit (*D*), a transmitter (*Tx*) and three receivers (*Rx*). The data are logged in real-time onboard ship. The system is dragged along the seafloor at speeds of 1–2 knots.

about 0.2 and 0.4 Ω m. In most cases, interstitial salinity has little variation. However, close to freshwater seeps or concentrated brine pools, the salinity dependence of resistivity may be more important.

3. Seafloor EM: essential physics

EM techniques for seafloor investigation rely on the length scale over which fields decay in a conductive medium, known as the skin depth. This depth, δ, is given in meters by:

$$503(\rho/f)^{1/2}$$

where ρ is the resistivity of the medium, and f is the frequency of transmission.

The seafloor is usually more resistive than seawater (e.g. Edwards and Chave, 1986; Chave et al., 1992; Cheesman et al., 1993), and is therefore characterized by greater skin depths. This means that when a seafloor source and receiver are separated by a lateral distance greater than a few skin depths in the ocean, a received signal will be dominated by the fields that have propagated through the seafloor. The frequencies and lateral separation of the source and receiver determine the geologic resolution. For the purposes of mapping shallow sedimentary resistivities, high frequencies of a few kHz are transmitted and short source–receiver separations (10–50 m) are required. A greater depth of sensitivity is obtained by increasing the source–receiver offset and decreasing the transmitted frequency, so that the offset is approximately equal to the skin depth in the seafloor, but is larger than the skin depth in the ocean.

In typical oceanic sedimentary environments, data are able to resolve structure to a depth of about half the maximum source–receiver offset. Frequency-domain EM provides far greater sensitivity to seafloor structure than standard direct-current (D.C.) resistivity methods adapted for the oceanic environment (Chave et al., 1992). With D.C., most of the applied current flows through the seawater and so even substantial changes in the seafloor resistivity have only a small effect on the seafloor voltages recorded.

A single measurement of the amplitude and phase of a transmitted magnetic field is sufficient to define an apparent seafloor resistivity, which is the uniform half-space that would produce the observed response. Each apparent resistivity is in some sense an average of the seafloor values over a local volume surrounding the source and receiver (discussed further in Section 7 below). By measuring apparent resistivities at different locations and at different source–receiver separations, it is possible to map the regional seafloor structure. In order to estimate porosity profiles, it is necessary to invert a series of measurements on different receivers at the same location.

EM propagation in the oceanic environment is a diffusive process, precluding the technique from obtaining the same kinds of detailed spatial im-

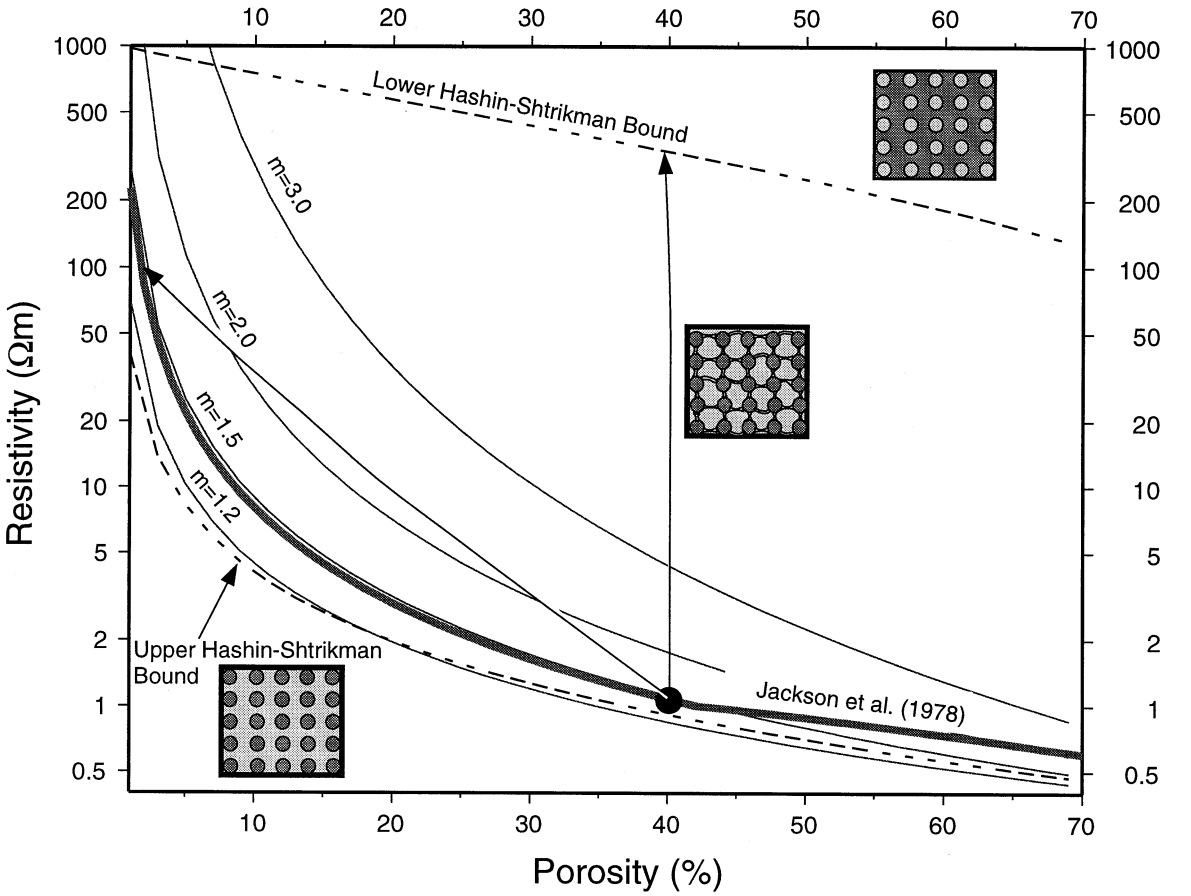

Fig. 3. Porosity–resistivity relationships for various distributions of a conductive fluid and resistive solid particles. Archie's law (Archie, 1942) is the most commonly used relationship and is plotted for several values of exponent *m* (1.2, 1.5, 2.0 and 3.0). Theoretical limits on the resistivity are given by the upper and lower Hashin–Shtrikman bounds (Hashin and Shtrikman, 1963). The upper bound considers spheroidal solid particles dispersed in the conductive fluid and is the optimal case of fluid connectivity. The lower bound has isolated fluid inclusions in a solid matrix and can have high porosities with little reduction in bulk resistivity. These extremes are shown in the cartoons. The average result of Jackson et al. (1978) demonstrates how the exponent in Archie's law is generally seen to increase with porosity for marine sediments. The two arrowed paths represent possible increases in resistivity resulting from the addition of either: (i) a very small amount of a third resistive phase (e.g., gas) which closes off conduction paths by linking grains; or (ii) a large volume of the third phase which is randomly distributed.

ages provided by seismic-reflection profiles. But the method does provide estimates of the bulk physical properties of the seafloor, both laterally and vertically, over depths ranges which seismic methods are not well equipped to address.

4. Equipment

The towed EM system used (Fig. 2) is compact and can be deployed from most coastal ships. The system has several components: a shipboard power supply and modem communications unit; a depressor weight containing a CTD sensor and a communications package; a transmitter; and three receivers. The system is towed along the seafloor using a 0.78″ multi-conductor cable, which carries power and a modem link from surface to seafloor, allowing the data to be logged in real time onboard ship.

The depressor weighs about 250 kg and its primary function is to ensure that the array following it is in contact with the seafloor. The CTD sensor

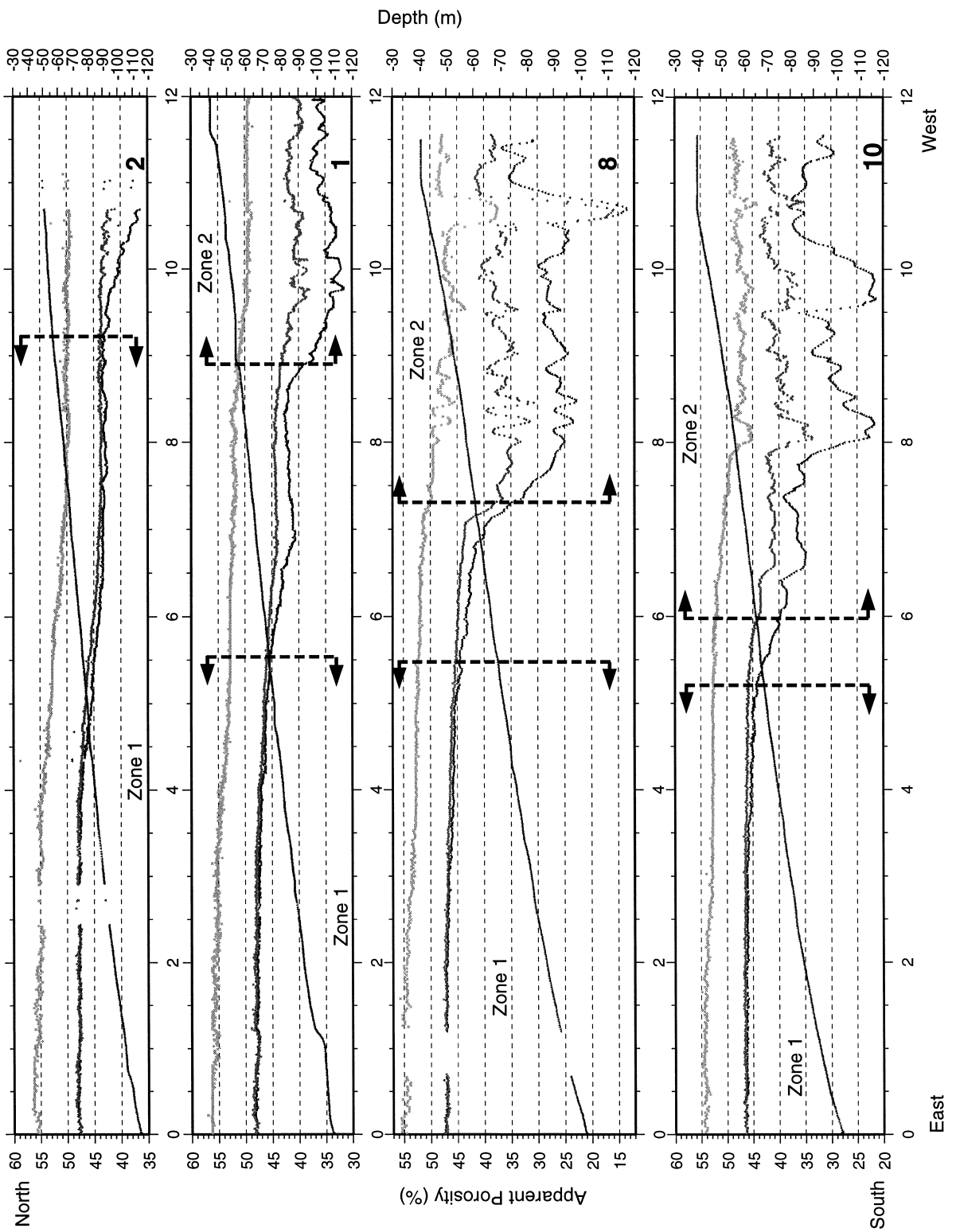
Depth (m)
Apparent Porosity (%)
North
South
East
West
Zone 1
Zone 2
2
1
8
10

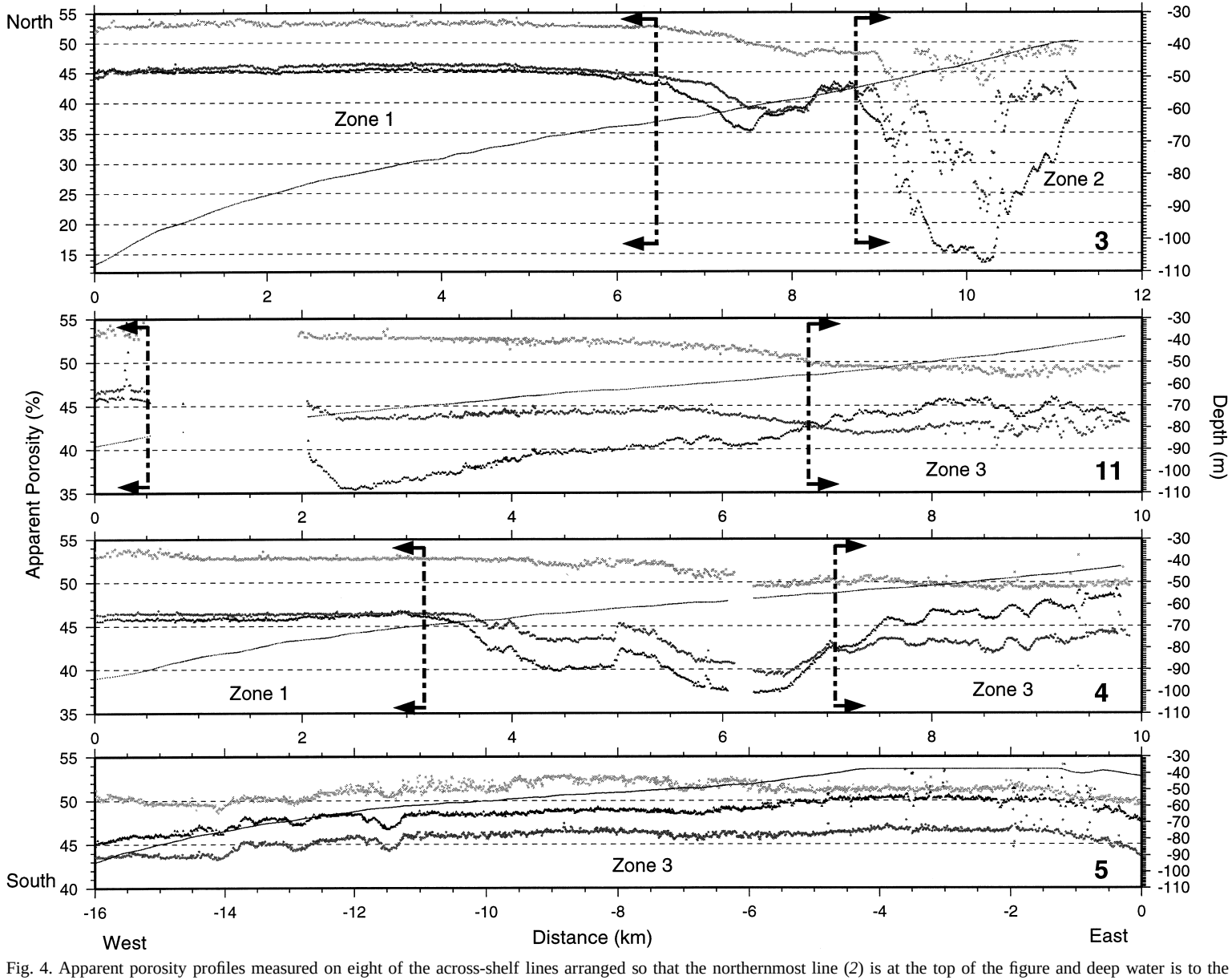

Fig. 4. Apparent porosity profiles measured on eight of the across-shelf lines arranged so that the northernmost line (*2*) is at the top of the figure and deep water is to the left. Data from the different zones shown in Fig. 1 are indicated. The lightest symbols are data from the 4-m receiver and average over the top 1–2 m of seafloor. Under normal circumstances the 40-m receiver measures the lowest apparent porosity, but in zone 3, the 13-m receiver recorded consistently lower values than the 40-m receiver. The data have been plotted as apparent porosity with distance along track from the first point on the line. The distances have been low-pass filtered so that a monotonic increase in distance along the track is obtained; this removes the effects of small deviations from a straight track line.

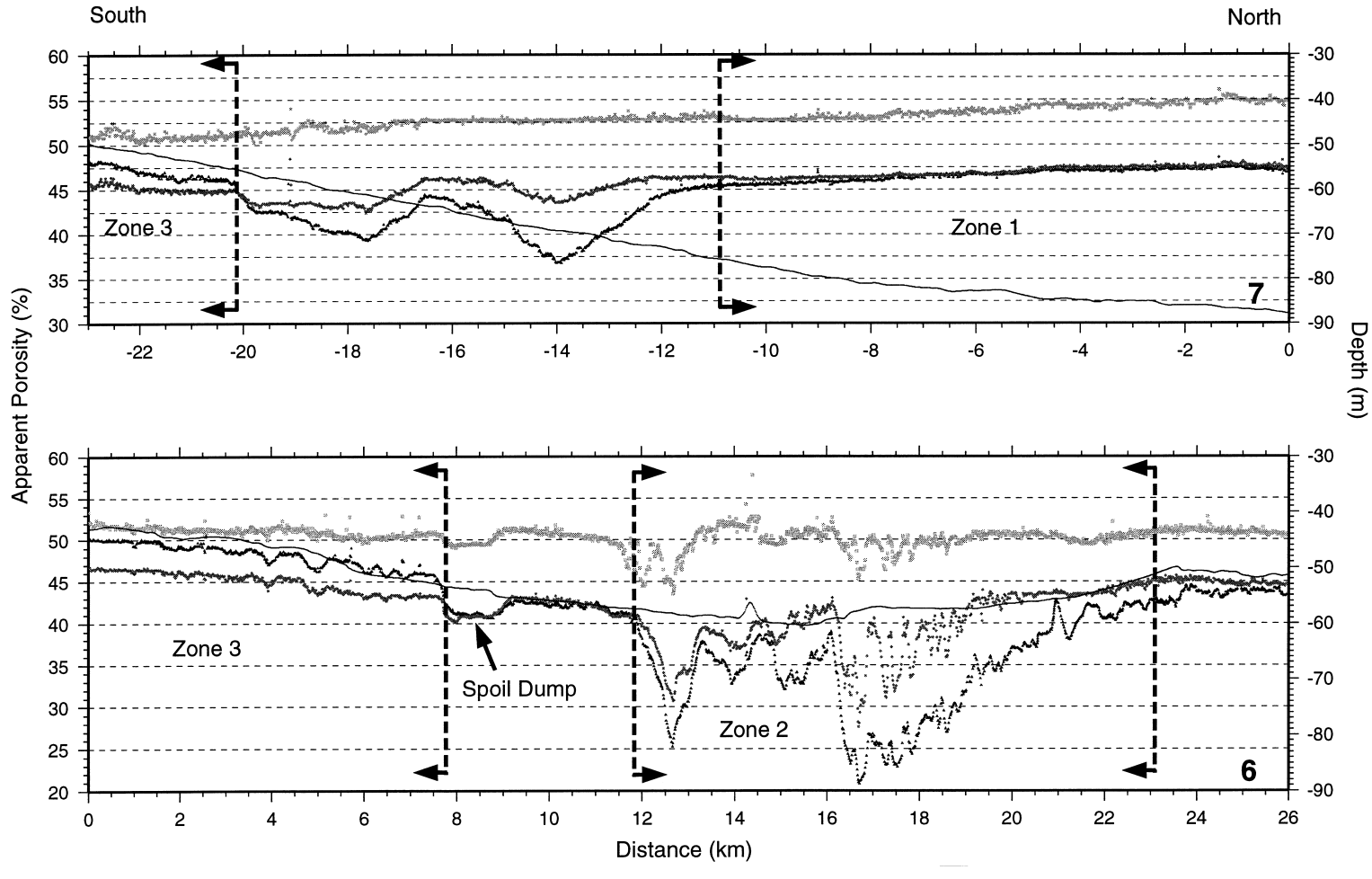

Fig. 5. Apparent porosity profiles measured on two north–south lines with the inner-shelf line (*6*) at bottom. Note that the surficial porosities on line 7 increase gradually from south to north (*zone 3* to *zone 1*).

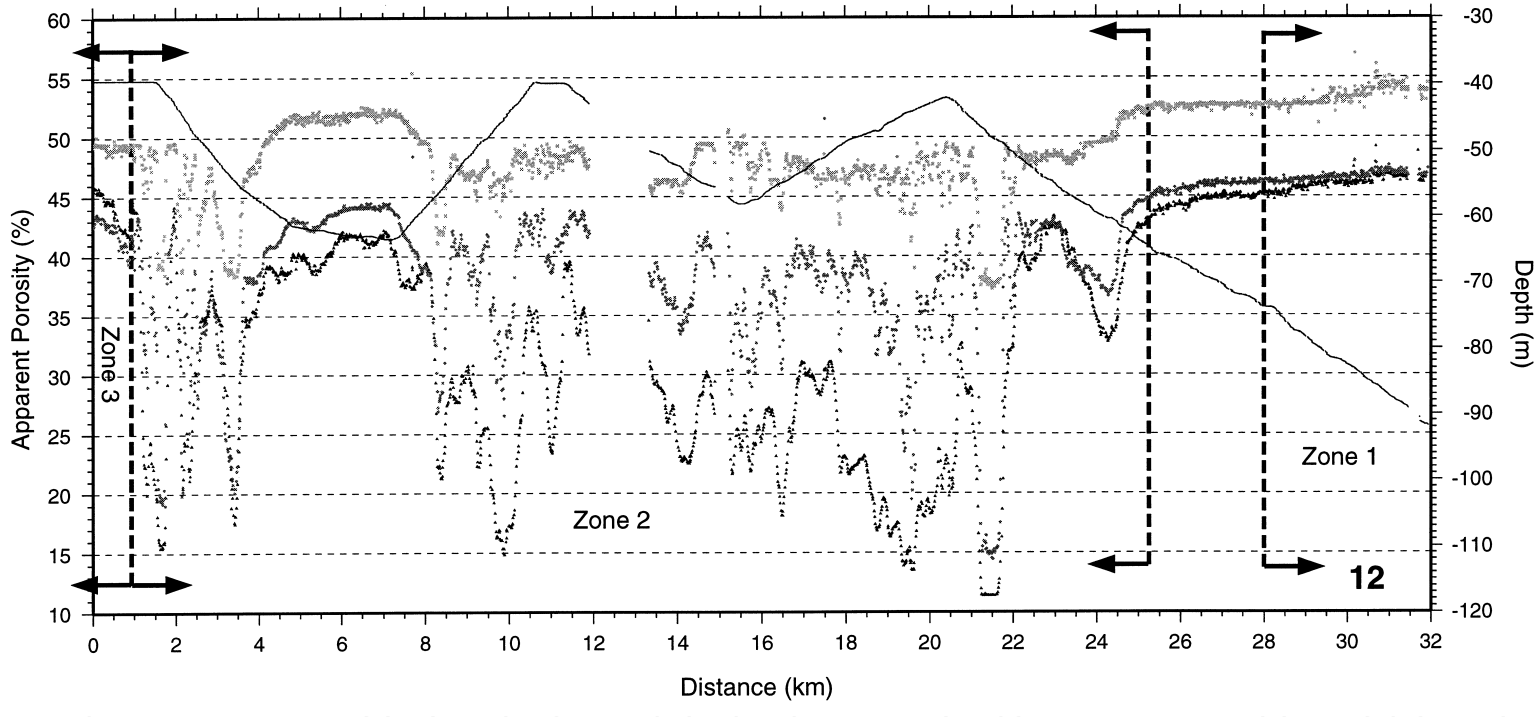

Fig. 6. The apparent porosities measured along line 12 through zone 2. This line shows the greatest spatial variability in porosity structure and also records the lowest values measured.

provides seawater conductivity values at each station. The transmitter is a magnetic coil housed in a rugged polyethylene cylindrical case, and weighs about 100 kg. The transmitter generates a series of distinct frequency sinusoid waveforms, the magnetic fields of which are recorded by the remote receivers. Frequencies range from 200 Hz for the farthest (40 m) receiver to 200 kHz at the closest (4 m) receiver.

The receivers are also magnetic coils and are linked by fibre optics to the depressor communications package. Each receiver remotely measures the amplitude and phase of the transmitted signal, which is passed through the communications link back to the ship. For each receiver, three appropriate frequencies are transmitted to provide enough information to obtain a resistivity–depth profile. The receivers are housed in Delrin cases for protection and are powered by separate battery packs.

Prior to surveying, the system is calibrated in the water column (in water depths greater than 100 m). This calibration provides estimates of instrumental uncertainties for amplitude and phase measurements at each receiver and frequency. Correlation of adjacent data points on the seafloor suggests that noise levels in the data are less than 1–2% in terms of apparent porosity, and noisy data are very easy to identify and reject. The system was towed at 1–2 knots. A set of measurements consists of logging amplitude and phase for each of the three receivers at three distinct frequencies, and takes on the order of 20 s, or approximately 10–20 m along track.

5. Survey

Over an 80-h period, we surveyed twelve lines across the shelf from water depths of 100 m to about 30 m (Fig. 1). Nine of the lines were in an across-shelf direction, two were coast-parallel cross lines, and the final line improved spatial coverage in an area of high structural variability. Lines were chosen where possible to be coincident with previous high-resolution Huntec seismic-reflection profiles completed during 1995 and 1996 surveys (Yun et al., 1999). The ship was navigated by differential GPS using the Cape Mendocino Coast Guard beacon as a reference station.

The recorded data and navigation files were merged, and an approximate seafloor position of the array calculated based on the ship's position, wire out, ship's speed and heading, and water depth; uncertainty in the array position is estimated to be 20–40 m.

The data were recorded in raw form as magnetic-field amplitude and phase, processed assuming a uniform seafloor half-space, and converted into apparent porosity values using Archie's law with an exponent of 1.8. While the apparent porosities are not true values, they are useful in a relative sense as indicators of structure, both along a line, and also with depth. Raw values of apparent porosity collected along each line are shown in Figs. 4–6. The profiles show measurements of apparent resistivity made on the three receivers. The 4-m receiver averages over the top 2 m or so of the seafloor and displays the highest apparent porosities. The final line, 12 (Fig. 6), shows the most dramatic lateral changes in apparent porosity and includes the lowest measurement of apparent porosity made by the system. Because porosity usually decreases with depth and the 40-m receiver measures porosity averaged (non-linearly) over the top 20 m or so of seafloor, apparent porosity values on this receiver are an overestimate of the true seafloor porosity at 20-m depth.

6. Data inversion

In order to obtain 'true' resistivity–depth profiles, data from adjacent stations are combined to give nine measurements of amplitude and phase. Spatially, this corresponds to binning data over a distance of about 50 m. These 18 values are inverted to find minimum structure-layered earth models, using both conventional Occam inversion methods (Constable et al., 1987) and L_1-norm minimization (Parker, 1994). The Occam method finds the smoothest model that satisfies the data (i.e., fits to a desired tolerance), while the L_1-norm inversion returns the model with the least number of layers required to satisfy the data.

The types of model returned by the Occam algorithm do not typically contain sharp discontinuities in resistivity, reflecting the diffusive nature of EM propagation through the seafloor. In a sedimentary depositional environment, we expect that the resistiv-

ity structure will exhibit layered characteristics and so we have emphasized the L_1-norm inversions in our analysis. However, where simple gravity-driven consolidation is important, smooth models may be more appropriate.

Errors in the measurements, which are important in deciding whether an inversion result is acceptable, are obtained during the calibration run and are based on the variance in repeat measurements at each receiver. Such errors will not account for other distortions in the data that may arise from two- or three-dimensionality in the seafloor structure (e.g., large lateral gradients in properties) or from other sources of instrumental noise such as the source or receiver leaving the bottom. For most of the data sub-sets examined, an acceptable level of misfit between the model response and data was achieved. However, in areas of large lateral gradients in structure, the assumption of one-dimensionality fails and a suitable model cannot be found.

7. Correlations with core porosity data

As a means of ground truthing our results, porosity values from four cores, which contain porosity information to a depth of around 4–6 m (C. Sommerfield, unpubl. data), were compared with apparent porosities measured by the 4-m receiver, and also against inverted resistivity profiles converted to porosities using Archie's law.

The apparent porosities measured closest to the locations of the cores are in good agreement with the core porosity averaged over the top 4 m. Profiles for two cores and appropriate models derived from EM data are shown in Fig. 7. The other two cores were at stations O90 and K110. O90 has an average porosity of 54% and a standard deviation of 6% over the top 4 m compared to an apparent porosity of 55% measured on the 4-m receiver. Values at K110 are 52% averaged over the core (standard deviation of 5%) and an apparent porosity of 54%.

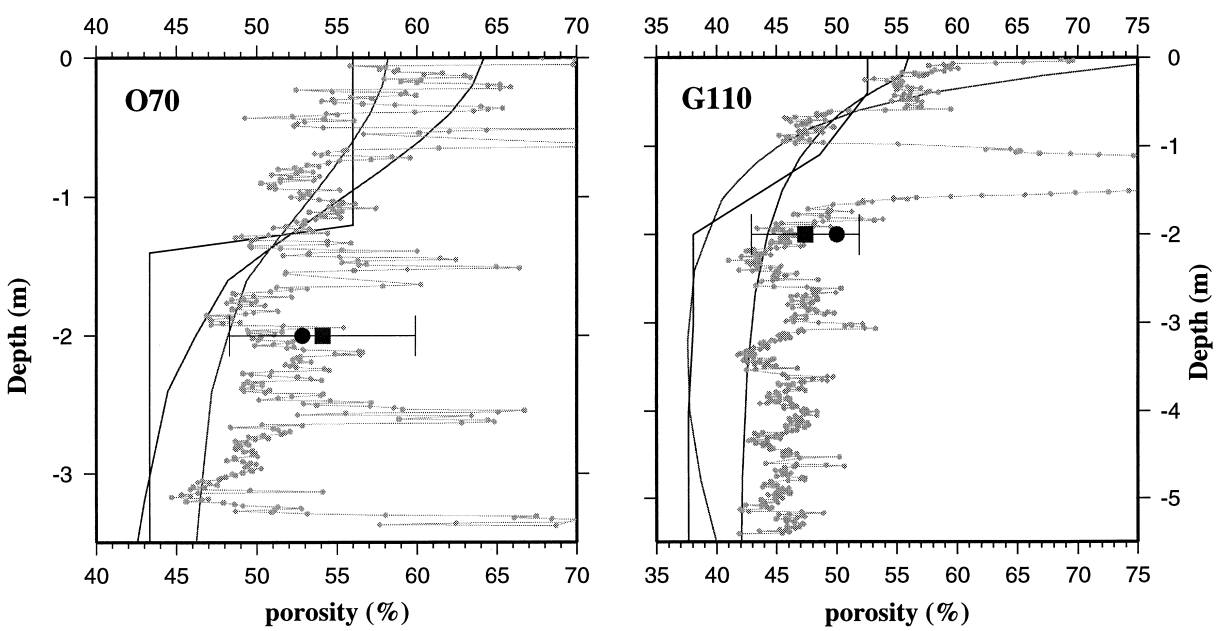

Fig. 7. Correlations between apparent and inverted porosity profiles and porosities measured from piston-core samples. Core O70 has a mean porosity (square) of 54% and a standard deviation of 4%. The closest measured apparent porosity on the 4-m receiver is 53% (circle). Values for core G110 are: mean 47% (not including the large gas-induced spike between 1 and 1.5 m depth); s.d. 5%; and apparent porosity 50%. Also shown are L_1-norm and 1st (flattest) and 2nd (least oscillatory) derivative smooth Occam models (Constable et al., 1987) derived from inverting data on all receivers (i.e., these models extend to 20 m below the seafloor). At station G110, the inversion results show the buried low-porosity layer starting at 2-m depth, just below where the core was disrupted by gas expansion. Gas distributed between depths of 2 m and ~6–7 m could be responsible for the low porosities (high resistivities).

The choice of 1.8 as an exponent in Archie's law is seen to be appropriate near the seafloor, given the good agreement between core and apparent porosity values. The shallow porosity profiles also were calculated using an exponent of 1.8. The comparison further demonstrates the near-seafloor resolution of the EM system. The inversion models resemble a low-pass-filtered version of the core profiles cut at a wavelength of ~1 m. Thus, the trend of porosity with depth is resolved, but not small wavelength features within the core. At station G110, a pocket of gas caused the core to expand, giving anomalously high porosities at 1-m depth. The non-invasive, in-situ nature of the EM system means that our measurements are not affected by disruption incurred by removal of the sample, such as re-mixing or gas expansion.

8. Interpretation

The data, in both raw form and after inversion (Fig. 8), identify three distinct facies across the Eel shelf (Fig. 1). The zones are defined by specific characteristics of the data, and obviously some of the boundaries of these zones (i.e., to the west of zone 1) are not defined by our data coverage. The intermediate regions between zones generally reflect consolidation-driven porosity–depth relationships and the data do not meet the criteria defining the three zones.

8.1. Zone 1

Found to the northwest of the entrance to Humboldt Bay, this region occurs between water depths of ~65–75 m and 100 m and is roughly coincident with that delineated by coring and bathymetry as the main depocenter for 1995 flood deposits (Wheatcroft et al., 1996). Zone 1 is defined by the similarity in data measured by the 13-m and 40-m receivers, indicating that there is little or no porosity gradient beneath the top 2 m. In waters shallower than 65 m, the upper layer decreases in apparent porosity and thickness, and the underlying layer becomes less homogeneous. Thus this region is characterized by a thin (~2 m), moderately high-porosity (45–60%) surface layer, which overlies a less porous (35–45%) and homogeneous substrate, uniform both laterally and vertically. The uppermost resistivity seems to decrease toward the base of small topographic slopes, probably indicating that these pockets are low-energy depositional environments containing recently deposited fine-grained sediments.

8.2. Zone 2

The second regime occurs on the inner shelf at water depths less than 60 m and between 40º49′N and 40º54′N. Here, we see high spatial variability in porosity structure, with apparent porosities less than 20% (in some places as low as 10% on the 40-m receiver), which are astonishing in a shelf sedimentary context. Line 12 (Fig. 6) exemplifies the degree of spatial variability observed.

Based on the raw apparent porosities and data inverted throughout this region, the lowest apparent porosities (less than 10%) are centered at 40º50.3′N, 124º15.7′N (Fig. 1), although there are several other regions within zone 2 with local apparent porosities less than 20% at 20-m depth. The low porosities extend upward to within a few meters of the seafloor, as witnessed by the fact that the 4-m receiver also measures locally low values (Fig. 6).

This region should be regarded as characterized by high resistivities rather than low porosities, because there are certain pore fluids and distributions of fluid that can have high resistivities at moderate to high porosities. There are several explanations for the high resistivities.

Seismic work shows that the depth to Tertiary and Cretaceous basement rocks of the Coastal Range is several hundred meters, far too deep to impact our measurements (Clarke, 1992; Yun et al., 1999). We also believe it unlikely that the sediments are highly consolidated. Instead, our explanations involve either fresh water or natural gas channeled to the seafloor through thrust faults: zone 2 lies between the axis of the Freshwater syncline to the north, and the Little Salmon fault to the south (Clarke, 1992).

Seismic-reflection work in the area documents substantial occurrences of gas across the shelf, and there is evidence of some gas seeping to the seafloor on the edge of zone 2 (Yun et al., 1999; M. Field and J. Gardner, unpubl. data). A gas seep within this region has been observed during ROV operations (Fig. 1; Jeff Borgeld, pers. commun., 1997).

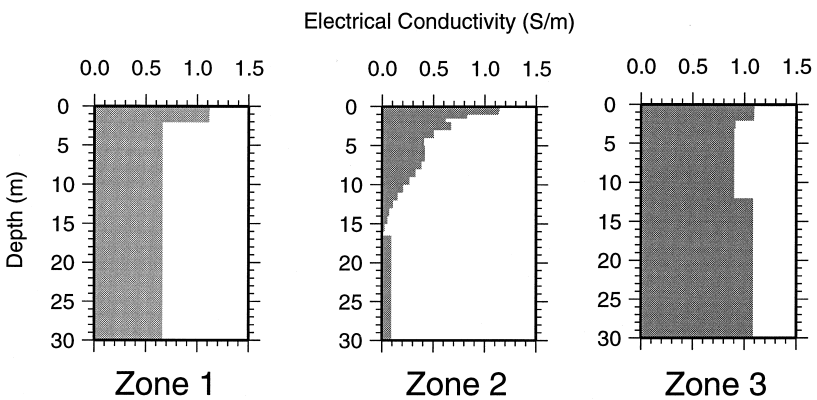

Fig. 8. Models derived from inverting data within each zone as labelled, showing conductivity (1/resistivity) as a function of depth. Zone 1 is characterized by a thin surficial layer overlying a uniform substrate. Zone 2 shows very steep gradients in conductivity, with very low values at depth. Zone 3 features a buried layer of lower conductivity than the overlying and underlying strata.

However, previous surveys in gas-prone areas show that seismic-reflection data are vastly more sensitive to the presence of small amounts of gas (less than 5% by volume) than are the bulk resistivities. EM surveys generally have shown little response in resistivity to the presence of gas (Cheesman et al., 1993). Recent resistivity logs of the Ocean Drilling Program, run through gas-rich sections, also have shown little response to the presence of free gas (Paull et al., 1996). Therefore, if our high resistivities are caused by gas, then there must either be substantial quantities present, or else some unusual facet to the gas distribution. How the resistivity is affected by gas depends on how it is distributed between sediment grains. If the gas is randomly placed, then the volume fractions needed to increase resistivity would equal the displaced volume of pore water. For example, a porosity of 40% and a measured apparent porosity of 5% would require 35% gas by volume. Such high volumes of gas are unlikely. If, however, the gas bubbles congregate in pore throats, blocking conduction paths through the sediment, then only very small volumes would be required to have a dramatic effect on the resistivity (Fig. 3).

The occurrence of carbonate cements in the seafloor sediment also could lower significantly the connectivity of pore fluids, and thus increase the seafloor resistivity. Carbonate cements are common where methane is carried to the seafloor, either by pore water or through a gas seep (e.g., Ritger et al., 1987; Hovland and Judd, 1988; Kulm and Suess, 1990), and are seen in abundance farther offshore where the Little Salmon fault channels methane and fresh water to the seafloor (D. Orange and S. Clarke, personal commun., 1997). Oxidation reactions precipitate carbonates in a confined region near the seafloor, so that normally only a thin crust of lithified material is formed. This is certainly true if the reaction is by bacterial oxidation of methane in an oxic environment (Ritger et al., 1987), and also seems to be the case if microbially mediated reactions are coupled with sulfate reduction (Reeburgh, 1980; Ritger et al., 1987). Where the gas seep is long lived, and sedimentary deposition is continually burying carbonates and raising the zone of sulfate oxidation of methane, then a thick sequence of carbonates could occur. Closure of pores and pathways, and the presence of a connected matrix (which is itself highly resistive), could easily raise the resistivities above those of normal sedimentary sequences. This model is speculative, largely because the time scales are not well known for carbonate formation in relation to sediment accumulation rate.

The conductivity of seawater is strongly dependent on salinity. Sediment filled with fresh water will be less conductive than that filled with seawater (Fig. 9). A reduction in salinity to 9.4 ppt (water conductivity of 1.0 S/m) means that a sediment with a true porosity of 40% would be predicted as having a porosity of only 17%. An even fresher pore water (0.72 ppt salinity) would cause us to predict a porosity less than 5% (over the range of values observed).

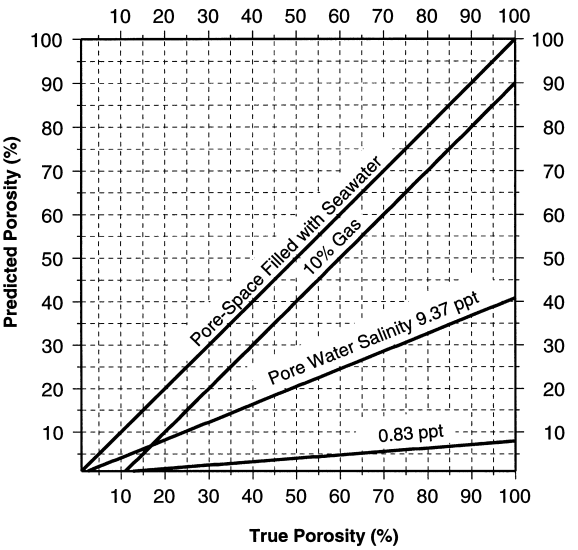

Fig. 9. The effect on predicted porosity that results from replacing 10% of the pore fluid with gas in a random distribution, and also by a fresh pore fluid with the salinities as labelled. See Fig. 3 for more details of how gas might influence resistivity.

Thus, fresh water discharged beneath zone 2 could also explain the observed resistivity pattern.

8.3. Zone 3

The third regime is roughly coincident with the region of low acoustic backscatter, interpreted as the signature of the Eel River delta (Goff et al., 1999), and begins ~5 km north of the Humboldt Bay entrance as a coast-parallel band a few kilometers wide. Opposite the bay entrance, the region widens and extends southwestward, to water depths of at least 100 m. This region shows an initial decrease in porosity over the top few meters, followed by a subsequent increase with depth.

The buried layer is of a lower porosity than the overlying and underlying strata by ~5–10%. The top of the layer is typically 5 m deep and 5–10 m thick. Toward the shelf edge, the layer increases in thickness and decreases in porosity. The buried resistive layer is present along the entire line, although the effect is most dramatic at the entrance to Humboldt Bay, where the 40-m and 4-m receivers essentially measure the same apparent porosity. For this to happen, the intermediate resistive zone may be acting as a permeability boundary, preventing the de-watering of the buried substrate. The buried layer points either to a change in depositional history on a time period of several decades, or to the effects of smaller quantities of trapped gas within the seafloor. A core sample from this region (in 110-m water depth) shows the effects of gas expansion raising the porosity on recovery (C. Sommerfield, unpubl. data) and seismic surveys also show gas throughout this region (Yun et al., 1999). This zone is coincident with low acoustic backscatter (Goff et al., 1999), which is not due to grain-size variations (Borgeld et al., 1999), but must be caused by another scattering mechanism. This is demonstrated also by the fact that surficial porosities in zone 3 (low backscatter) are lower than in zone 1 (high backscatter) and increase from south to north (Fig. 5). While the effects of a few percent trapped gas could cause the reduction in apparent porosity at depth, the consistency and abrupt boundaries of the buried layer point to a structural explanation, possibly a change in depositional history across the region.

9. Summary

We have collected EM data that are complementary to data from other geophysical techniques, and which provide a unique means of mapping spatial variations in physical properties over areas that would take far too long to cover by coring. Porosities obtained are consistent in the uppermost 4–6 m with those measured in adjacent piston cores.

Our data reveal a high degree of variability in underlying porosity structure that is not apparent from surficial mapping. We identify three distinct environments. One is a mid-shelf depocenter for fine-grained material originating from local river systems. The second region shows dramatic variability in resistivity structure, with extremely high resistivities for a sedimentary environment. We propose three possible explanations for these high resistivities: freshwater discharge from the continent; natural gas; or a substantial sequence of methane-derived carbonates. These three explanations are not mutually exclusive: the presence of fresh water may serve to increase gas production, and without the gas seepage there can be no carbonate deposition. These models remain

speculative due to a lack of core samples, but can be easily tested in the future by coring and in-situ resistivity measurements. The third zone lies within the Eel River delta and shows a buried layer of lower porosity sandwiched between higher-porosity units. This layer probably indicates change in depositional patterns in the delta, but could be due to a few percent gas trapped within the seafloor.

Acknowledgements

We thank the crew of the R/V *William McGaw*, whose skill and enthusiasm made for a productive cruise. We also thank Eben Franks, Fred Thwaites and Bill Shaw for their help during the survey. The EM system is owned and operated by the Geological Survey of Canada. Numerous discussions with Neal Driscoll as well as with Janet Yun, John Goff, Dan Orange, Sam Clarke, Jean Whelan and Jeff Borgeld have helped us in our final interpretations. Chris Sommerfield is thanked for providing the unpublished porosity profiles. Mike Field and Jim Gardner provided raw Huntec profiles. Constructive reviews provided by Charlie Paull, Larry Mayer, Michael Richardson, Chuck Nittrouer and one anonymous reviewer without doubt improved the clarity and content of the paper. This project was funded by ONR grant N00014-96-1-0843 through the office of Dr. J. Kravitz.

References

Andrews, D., Bennett, A., 1984. Measurements of diffusivity near the sediment–water interface with a fine scale resistivity probe. Geochim. Cosmochim. Acta 45, 2169–2175.

Archie, G.E., 1942. The electrical resistivity log as an aid in determining some reservoir characteristics. J. Pet. Technol. 5, 1–8.

Borgeld, J.C., Hughes Clarke, J.E., Goff, J.A., Mayer, L.A., Curtis, J.A., 1999. Acoustic backscatter of the 1995 flood deposit on the Eel shelf. Mar. Geol. 154, 197–210.

Chave, A.D., Constable, S.C., Edwards, R.N., 1992. Electrical exploration methods for the seafloor. In: Nabighian, M.N. (Ed.), Electromagnetic Methods in Applied Geophysics, II. Society for Exploration Geophysicists, Tulsa, OK, pp. 931–966.

Cheesman, S.J., Law, L.K., St. Louis, B., 1993. A porosity survey in Hecate Strait using a seafloor electro-magnetic profiling system. Mar. Geol. 110, 245–256.

Clarke, S.H., 1992. Geology of the Eel River basin and adjacent region: implications for late Cenozoic tectonics of the southern Cascadia subduction zone and Mendocino triple junction. Am. Assoc. Pet. Geol. Bull. 76, 199–224.

Constable, S.C., Parker, R.L., Constable, C.G., 1987. Occam's inversion: a practical algorithm for generating smooth models from electromagnetic sounding data. Geophysics 52, 289–300.

Edwards, R.N., Chave, A.D., 1986. A transient electric dipole–dipole method for mapping the conductivity of the seafloor. Geophysics 51, 984–987.

Evans, R.L., 1994. Constraints on the large scale porosity of young oceanic crust from seismic and resistivity data. Geophys. J. Int. 119, 869–879.

Field, M.E., Gardner, J.V., Drake, D.E., Cacchione, D.A., 1987. Tectonic morphology of offshore Eel River basin, California. In: Schymiczek, H., Suchsland, R. (Eds.), Tectonics, Sedimentation and Evolution of the Eel River and other Coastal Basins of Northern California. San Joaquin Geol. Surv. Misc. Publ. 37, 41–48.

Goff, J.A., Orange, D.L., Mayer, L.A., Hughes Clarke, J.E., 1999. Detailed investigation of continental shelf morphology using a high-resolution swath sonar survey: the Eel margin, northern California. Mar. Geol. 154, 255–269.

Hashin, Z., Shtrikman, S., 1963. A variational approach to the theory of effective magnetic permeability of multiphase materials. J. Appl. Phys. 33, 3125–3131.

Hovland, M., Judd, A.G., 1988. Seabed Pockmarks and Seepages; Impact on Geology, Biology and the Marine Environment. Graham and Trotman, London, 293 pp.

Jackson, P.D., Taylor-Smith, D., Stanford, P.N., 1978. Resistivity–porosity–particle shape relationships for marine sands. Geophysics 43, 1250–1268.

Kulm, L.D., Suess, E., 1990. Relationships between carbonate deposits and fluid venting: Oregon accretionary prism. J. Geophys. Res. 95, 8899–8915.

Madden, T.R., 1976. Random networks and mixing laws. Geophysics 41, 1104–1125.

Nesbitt, B.E., 1993. Electrical resistivities of crustal fluids. J. Geophys. Res. 98, 4301–4310.

Nittrouer, C.A., 1999. STRATAFORM: overview of its design and synthesis of its results. Mar. Geol. 154, 3–12.

Nittrouer, C.A., Kravitz, J.H., 1996. STRATAFORM: a program to study the creation and interpretation of sedimentary strata on continental margins. Oceanography 9, 146–152.

Parker, R.L., 1994. Geophysical Inverse Theory. Princeton Univ. Press, NJ, 386 pp.

Paull, C.K., Matsumoto, R., Wallace, P.J. et al., 1996. Proceedings of the Ocean Drilling Program, Initial Results, 164. Texas A&M University, College Station, TX, 623 pp.

Perkin, R.G., Lewis, E.L., 1980. The practical salinity scale 1978: fitting the data. I.E.E.E. J. Oceanogr. Eng. 5, 9.

Quist, A.S., Marshall, W.L., 1968. Electrical conductances of aqueous sodium chloride solutions from 0° to 800°C and at pressures to 4000 bars. J. Phys. Chem. 71, 684–703.

Reeburgh, W.S., 1980. Anaerobic methane oxidation: rate depth distributions in Skan Bay sediments. Earth Planet. Sci. Lett. 47, 345–352.

Ritger, S., Carson, B., Suess, E., 1987. Methane-derived authigenic carbonates formed by subduction-induced pore-water expulsion along the Oregon–Washington margin. Geol. Soc. Am. Bull. 98, 147–156.

Schmeling, H., 1986. Numerical models on the influence of partial melt on elastic, anelastic and electrical properties of rocks, part II. Electrical conductivity. Phys. Earth Planet. Inter. 43, 123–136.

Wheatcroft, R.A., Borgeld, J.C., Born, R.S., Drake, D.E., Leithold, E.L., Nittrouer, C.A., Sommerfield, C.K., 1996. The anatomy of an oceanic flood deposit. Oceanography 9, 158–162.

Yun, J.W., Orange, D.L., Field, M.E., 1999. Subsurface gas offshore of northern California and its link to submarine geomorphology. Mar. Geol. 154, 357–368.